Multicell accelerating structure driven by a lens-focused THz pulse

S. Antipov,[1] S. V. Kuzikov,[1,*] and A. A. Vikharev[2]
[1]*Euclid Techlabs LLC, Bolingbrook, Illinois 60440, USA*
[2]*Institute of Applied Physics, Russian Academy of Sciences, Nizhny Novgorod, 603950, Russia*

(Received 15 December 2020; revised 25 November 2021; accepted 9 August 2022; published 7 September 2022)

Recently, gradients on the order of 1 GV/m have been obtained with single-cycle (~1 ps) THz pulses produced by the conversion of high peak power laser radiation, in nonlinear crystals (~1 mJ, 1 ps, up to 3% conversion efficiency). Such high intensity radiation can be utilized for charged particle acceleration. For efficient acceleration, a large number of accelerating cells have to be stacked together with delay lines in order to provide proper timing between accelerating fields and moving electrons. Additionally, THz pulses in individual cells need to be focused transversely to maximize the accelerating gradient. This focusing is currently done by the tapering of the waveguide. In this paper, we propose instead to use dielectric lenses for the robust focusing of THz pulses in accelerating cells. Each lens is made from the same material as the delay line in a monolithic unit. We have fabricated prototype units from quartz and silicon. Such an approach simplifies the fabrication and alignment of the multicell accelerating structure. We present a design in which a 100 microJoule THz pulse produces a 600 keV energy gain in a 5-mm long 10-cell accelerating structure for an ultrarelativistic electron. This approach can be extended to nonrelativistic particles.

DOI: 10.1103/PhysRevAccelBeams.25.091302

I. INTRODUCTION

The progress of particle and accelerator physics relies on the achievement of high gradient charged particle acceleration [1–5]. Record gradients above 1 GV/m are being produced in laser plasma wakefield acceleration (LPWA) and beam driven plasma wakefield acceleration (PWFA). Traditional technology reaches the level of 100 MV/m in normal conducting microwave accelerating cavities, in which charged particles gain energy surfing the electromagnetic wave with a frequency range of 1–10 GHz [1,2]. Any further progress in normal conducting structure gradients has been limited due to breakdown and thermal fatigue effects associated with pulsed heating [6–12]. Threshold values of surface electromagnetic fields strongly depend on the duration of material exposure to these extreme conditions. Experimental statistics [8,11,13] yield the following scaling law for the surface electric E_s field as a function of the exposure time τ (microwave pulse length): $E_s^p \tau = \text{const}$, $p = 5$–6. It is also well-established that the breakdown threshold correlates with pulsed heating of accelerating structure ΔT, which is determined by the surface magnetic field H_s: $T \sim H_s^2 \sqrt{\tau} = \text{const}$ [11]. A few theoretical models have been developed to explain this behavior [14,15].

These experimental dependencies strongly suggest that the gradient can be further increased if the pulse length is reduced. To take this idea to its ultimate limit, one can imagine acceleration by a single-cycle electromagnetic pulse (Fig. 1). A two-beam accelerating scheme can be proposed, similar to CLIC [16], in which a high charge, so-called "drive" beam is used to produce an electromagnetic pulse that in turn is used to accelerate the main beam at an extremely high gradient. Production of short intense pulses by the means of transition radiation has been demonstrated at SLAC [17]. The power extraction from the drive beam can be very efficient as is typical for vacuum electronic devices. The process of acceleration, as is shown in this paper, can be also efficient and occur at a high gradient. What is particularly attractive is that proof of principle experiments can be done at the university scale, because there is an alternative method to produce a short THz pulse. As it was recently demonstrated, intense, short picosecond pulses can be generated by high power lasers in nonlinear crystals via optical rectification. The energy in such pulses can be as high as 1 milliJoule resulting in few gigavolts per meter fields [18–20]. One can generate several such pulses with a time delay and use them in an accelerating cavity similarly to microwave acceleration providing a long interaction length [21,22]. However, a single short pulse can also be used. Such picosecond pulses are broadband

*s.kuzikov@euclidtechlabs.com

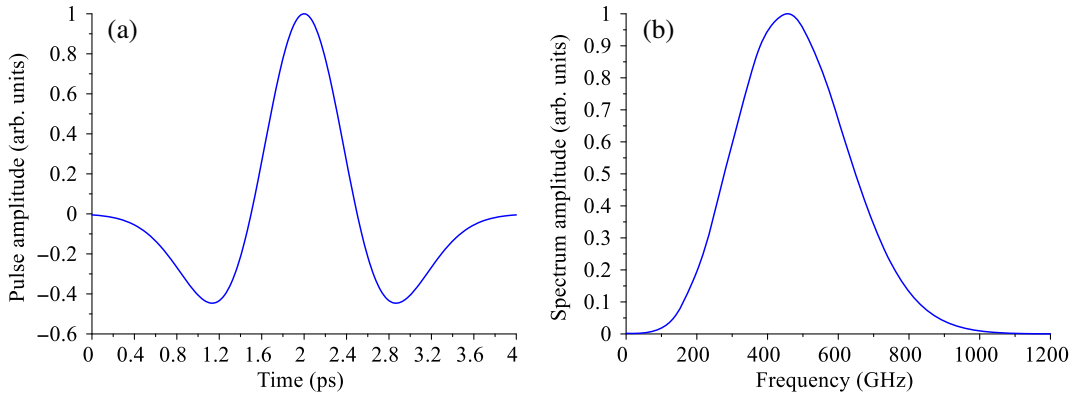

FIG. 1. Single-cycle THz pulse shape (a) and spectrum (b).

(Fig. 1), with a spectrum covering the range from 0.1 to a few THz. For this reason, such pulses are commonly referred to as THz pulses. In the case of short pulses, the accelerating structure must be extremely broadband, which is completely different from standard arrays of coupled resonators. A new approach is required for an accelerating structure design to facilitate efficient energy transfer from a broadband picosecond pulse to a charged particle.

In one of the first experiments in THz acceleration, electrons were accelerated by a focused THz pulse [23]. A short interaction length of about 300 μm resulted in a modest energy gain of a few keV. For a given THz pulse with fixed energy, the highest accelerating gradient can be achieved if this whole energy is focused on a single accelerating cell. When the same pulse is split to feed N separate accelerating cells, the gradient in each cell decreases as $\sim\sqrt{N}$. However, the total energy gain by a charged particle grows as $\sim\sqrt{N}$, being a product of gradient and structure length. For this reason, it is beneficial to consider an extended interaction of a THz pulse with the charged particle in multicell accelerating structures with $N \geq 10$. However such multicell accelerating structures need to maintain synchronization between the THz pulse and electron. A common approach addressing this requirement has been published elsewhere [24–26].

In the illustration presented in Fig. 2, a picosecond pulse is fed symmetrically from two sides into an array of accelerating cells along the x-axis. Each accelerating gap has a dielectric delay line with its length tuned to maintain the synchronization between the THz pulse and electrons travelling in Z-direction. The use of dielectrics of increased thickness along the length of the accelerating array ensures that electrons pass each accelerating gap at the maximum electric field. In the case of an ultrarelativistic electron beam that moves with constant velocity virtually equal to the speed of light, lengths of delay inserts decrease correspondingly to maintain synchronization between the particle and the THz pulse: $\Delta = \frac{p}{\sqrt{\varepsilon}-1}$, here ε is the dielectric permittivity of the delay material, p is a period of the structure, and Δ is the delay line length change. The acceleration of nonrelativistic particles is done in the same fashion and was experimentally demonstrated at a small scale [24,25]. These experiments demonstrated 70 keV energy gain for electrons with an initial energy of 55 keV and in an accelerating gradient of 200 MV/m. In this case, the delay line length is chosen to match the changing velocity of a nonrelativistic particle which is accelerated by the THz pulse.

Delay lines must be broadband enough so that there is no picosecond pulse degradation due to waveguide dispersion. This is true for large waveguide apertures. However, it also

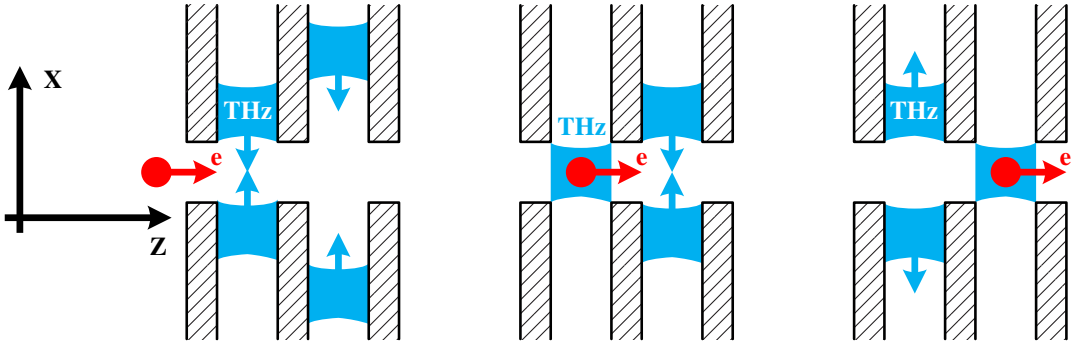

FIG. 2. Timing of THz pulses in the structure for acceleration synchronism.

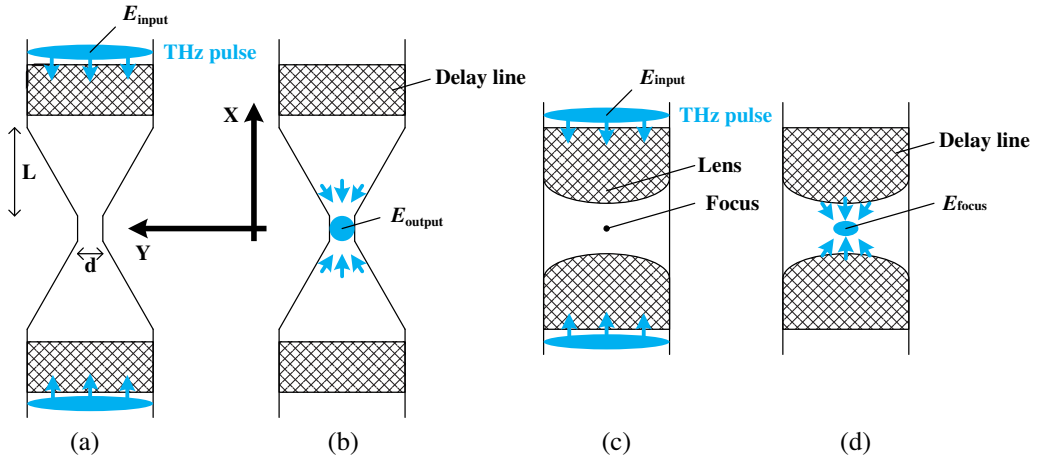

FIG. 3. Transverse focusing by tapering of the waveguide. THz pulse entering waveguide (a) THz pulse focused on the accelerating gap (b). Transverse focusing by a lens. THz pulse entering waveguide (c). THz pulse focused on the accelerating gap (d).

means that the THz pulse occupies a large volume in the accelerating gap and the gradient is relatively low. To increase the gradient, the THz pulse needs to be focused on the y axis. To achieve that, a horn-like geometry has been proposed and demonstrated [25] [Figs. 3(a) and 3(b)]. This solution is limited by the waveguide dispersion and leads to pulse broadening and field structure distortion. For an accelerating structure with a large number of cells ($\sim$10) this will lead to electron beam quality degradation.

In this paper, we use an alternative to the horn-like dispersive tapered waveguide—a monolithic-unit delay line with a lens [Figs. 3(c) and 3(d)] to increase the accelerating gradient in the gap. A dielectric lens made of a dispersionless material is a broadband element and does not produce noticeable losses and distortions of the accelerating field [27–29]. The accelerating gradient can be increased multiple times due to the focusing of the THz pulse. Below, we will compare the dielectric lens with the tapered waveguide. We will present a multicell accelerating structure based on this geometry. A prototype delay line with lenses based on this dielectric lens concept has been fabricated by laser microfabrication.

II. COMPARISON OF THE WAVEGUIDE TAPERING AND LENS FOCUSING

We performed extensive parametric studies of focusing broadband THz pulses by a lens and concentrating them with tapered waveguides. In this study, we assume that the THz pulse enters the accelerating structure with a constant phase, i.e., as a plane wave. In the experiments, the THz pulse is typically prefocused on the accelerating structure. These parameters vary from experiment to experiment and have been rarely discussed in previously published papers in detail. This prefocusing is done with large focal length mirrors or lenses, hence the beam is mildly converging. The prefocused beam passing through delay lines of different lengths followed by a focusing element (lens or tapered waveguide) experiences different focusing. Ideally, one would want to form a THz pulse with a constant phase to avoid these effects in the multicell accelerating structure. In this paper, we compare a lens and a tapered waveguide for the case of a plane wave.

Focusing by a lens [Figs. 3(c) and 3(d)] is a quasi-optic solution. It allows the focusing of broadband THz radiation into the path of a charged particle. The shape of the single-sided one-dimensional lens is a hyperbola [30] of eccentricity n and origin in one focus. In polar coordinates (r,θ), this contour can be written as: $r=(n-1)f/(n\cos\theta-1))$, where f is the focal length and n is the index of refraction of the material. Concentrating the THz pulse by a tapered waveguide suffers from dispersion. When the waveguide becomes narrow, different portions of the pulse's spectrum have different group velocities, leading to pulse broadening.

In our simulations, we use a broadband THz pulse with 1 picosecond duration (Fig. 1). In practice, such short THz pulses produced by short laser beams in nonlinear crystals have a duration and bandwidth depending on the THz generation setup parameters. It is typical that the bandwidth for THz pulses is slightly wider than 1 THz. We limited ourselves to 1-THz bandwidth to keep computational time reasonable. Figure 4 shows our simulation of a picosecond pulse focused by a quartz lens (snapshots of the electric field in time). Figure 4(d) shows a high peak field when the THz pulse is focused. We also simulated focusing with a lens made out of another excellent THz material—high resistivity silicon. The quartz lens exhibits no change in the time structure of the THz pulse [Fig. 7(a)].

To compare the lens with a tapered waveguide, we will use a ratio of the maximum field in focus [Fig. 4(d)] to the amplitude of the field at the input of the waveguide [Fig. 4(a)]. This field enhancement parameter, $E_{\mathrm{focus}}/E_{\mathrm{input}}$, quantifies focusing in parametric scans. For a waveguide

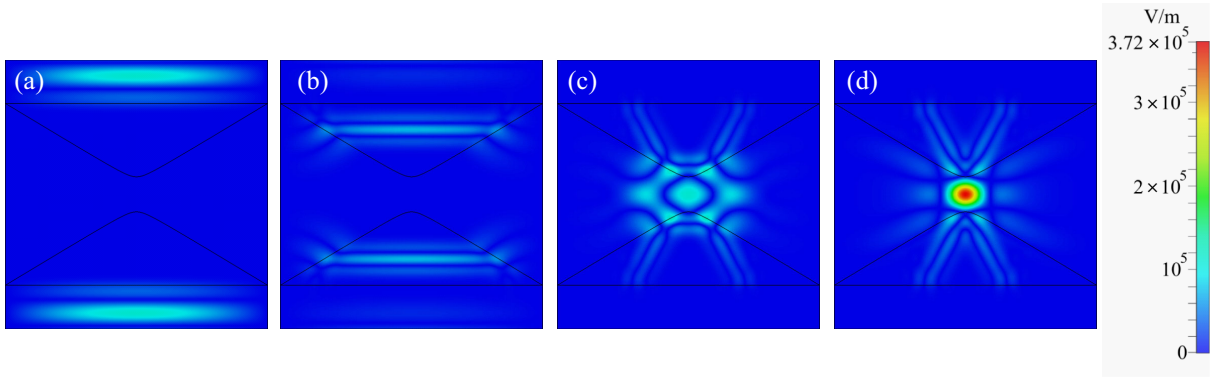

FIG. 4. E-field distributions at the quartz lens while focusing the short THz pulse. From the time when the THz pulse arrives at the lens, $t = 2.6$ ps (a), focusing begins, $t = 5.6$ ps (b), THz pulse is close to being focused, $t = 8.6$ ps (c), and maximum of focusing, $t = 9.6$ ps (d).

with a 3-mm aperture (Table I), field enhancement depends on the focal length of the lens (Fig. 5). It is beneficial to use a short focal length for high field enhancement. However, when it is too short, aberrations prevent efficient focusing. For quartz lenses, we can reach a field enhancement factor of 3 at a focal distance of 0.15 mm. Silicon has a smaller field enhancement maximum. This is because it has a larger dielectric constant than quartz which leads to a larger reflection at the vacuum-dielectric interface.

The tapered waveguide is a viable alternative for transverse focusing. In Ref. [24], a 30 μJ THz pulse was used in a three-cell accelerating structure to produce a 30-keV energy gain. By introducing a tapered waveguide [25] the total energy gain increased over two-fold to 70 keV.

To compare the tapered waveguide with the lens we simulated the same input waveguide dimensions along with the same delay lines. Reflection from the delay line, the taper, and ohmic losses were included in this calculation. One clear difference between the lens and the tapered waveguide is the broadening of the pulse due to waveguide dispersion (Fig. 6).

In Fig. 7, the electric field time dependence is shown at the entrance of the waveguide, the focus of the lens, and in the middle of the tapered section of the waveguide. When focused by the lens the THz pulse does not change its time structure. Focusing by the tapered waveguide exhibits broadening. This time structure is sensitive to the taper parameters.

We varied the length of the taper, L, and the width of the narrowest part, d. The result of a parametric scan is presented in Fig. 8. We observe that, despite the dispersion, field enhancement can reach values comparable to the ones from the dielectric lens. When the taper is too short, part of the broadband pulse gets reflected and does not contribute to the intensity at the focus. Longer tapers improve the reflection situation. However, in a long taper, dispersion of the THz pulse leads to different portions of the spectrum arriving at the focus at different times, reducing field enhancement. Maximum enhancement is observed when these two effects balance.

The parametric scan results from Fig. 8 show a strong dependence of field enhancement on waveguide parameters. This has an important practical aspect. Inevitable fabrication errors in the manufacturing process lead to

TABLE I. Parameters of THz accelerating structures.

Parameters	Silicon	Quartz
Number of cells	10	10
Dielectric permittivity	11.9	3.75
Cell length (mm)	0.2	0.2
Beam pipe diameter (mm)	0.1	0.1
Focal length (mm)	0.2	0.2
Iris thickness (mm)	0.2	0.2
Width (mm)	3	3
Length (mm)	4	4

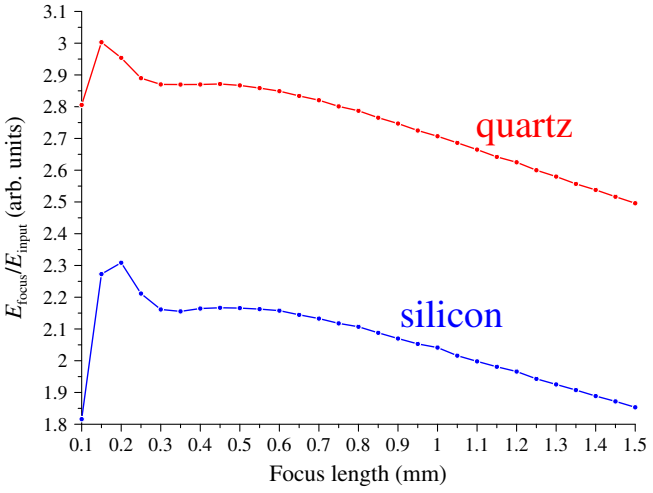

FIG. 5. Field enhancement at the focal plane of the lens for different lens materials. Red dashes are for quartz and blue for silicon.

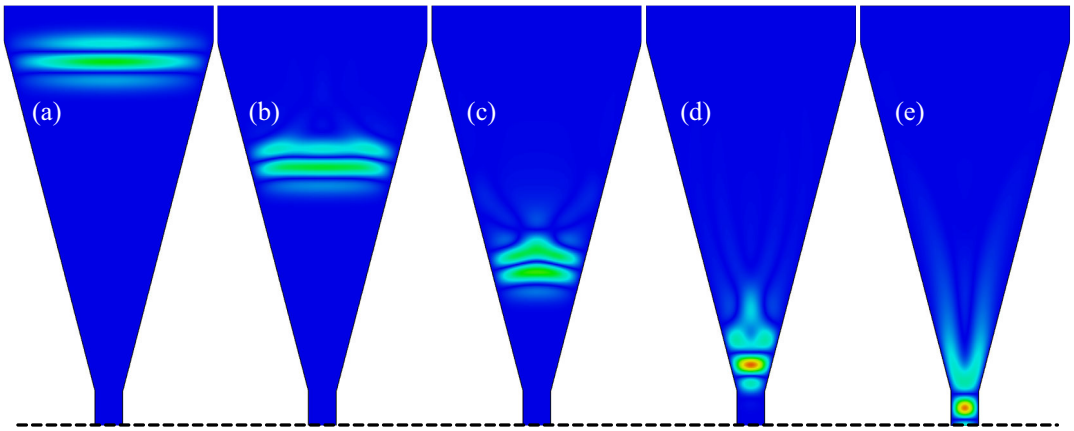

FIG. 6. E-field distributions of the THz pulse focusing in a tapered waveguide at consecutive time steps from the time the pulse arrives at the horn (a) to when it is focused (e).

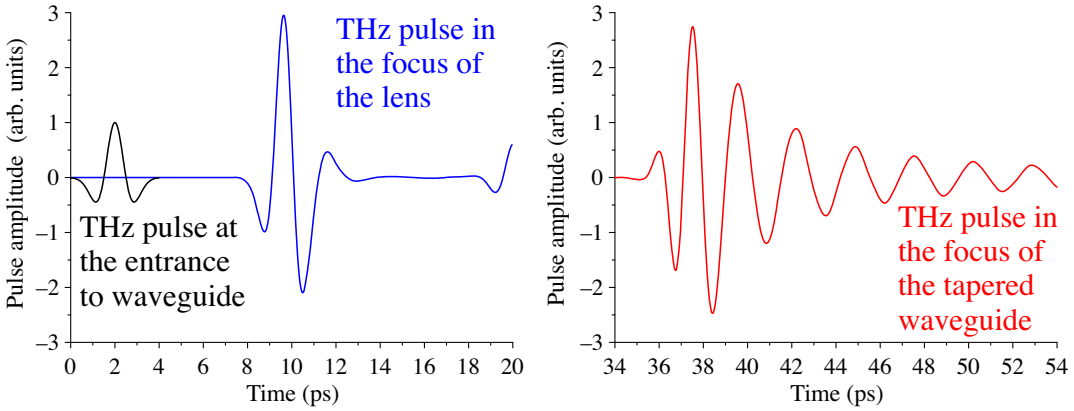

FIG. 7. Time structure of the initial THz pulse (black), the electric field at the focus of the lens (blue), and the electric field in the center of the tapered waveguide (red) for optimal focusing parameters, $L = 5$, $d = 0.4$ mm. Both plots are on the same time scale (20 ps) and are normalized to the amplitude of the incoming THz pulse.

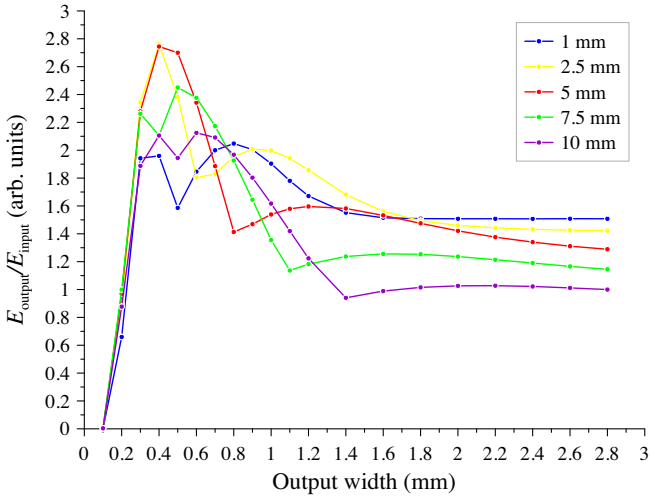

FIG. 8. Field enhancement at the focus of the tapered waveguide as a function of the width d and length L.

significant changes in field distribution. When stacking ten or more accelerating cells together, it is important that the electromagnetic performance of the structure is robust, i.e., does not change much even if fabrication errors are present. Due to the dispersion-less nature of lens focusing, we expect that a multicell accelerating structure with lenses would be less sensitive to small misalignments and fabrication errors. We show below that delay lines paired with lenses can be cut out of quartz or silicon by a standard laser router for wafer cutting.

III. ACCELERATING STRUCTURE DESIGN

We designed a full-featured 10-cell accelerating structure based on delay lines with focusing lenses. This multicell structure is fed symmetrically (Fig. 9 from top and bottom) by two identical short THz pulses. Each cell has a broadband dielectric delay line. If the electron beam is shorter than the length of the THz pulse, it can be accelerated provided that proper delays between cells are realized.

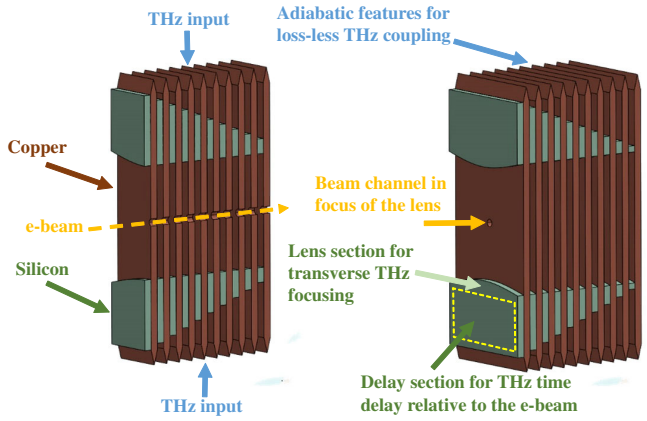

FIG. 9. Sketch of a multicell broadband accelerating structure based on dielectric delay sections and lenses.

The number of accelerating cells is limited by the dispersion of dielectric properties of the delay-line material and the wide waveguide dispersion, which may lead to THz pulse shape distortion. For a broadband THz pulse, the choice of delay-line dielectric is more important, as the dielectric constant should not have much variation over the wide range of frequencies corresponding to the THz pulse (Fig. 1). For the practical structure design presented here, we chose quartz as the delay line and lens material. High resistivity silicon can also be used in a similar fashion. These materials have a minimal frequency dispersion in the frequency range of interest for this application [31] for both indexes of refraction and power loss. A short, picosecond THz pulse propagating in 2-mm long silicon delay line experiences a 1% power loss. Quartz is a bit more lossy having 4% power loss in the same conditions.

While the absence of dielectric dispersion is the main criterion of choice for the delay line/lens material, another consideration is important. The larger the dielectric constant, the higher the reflection at the vacuum-dielectric boundary. Reflected power does not contribute to gradient and should be minimized. The reflection coefficient is calculated as

$$R = \frac{\sqrt{\varepsilon} - 1}{\sqrt{\varepsilon} + 1} \tag{1}$$

In the case of a quartz ($\varepsilon = 4.2$) delay line, the loss of power due to reflection is about 11%. In the case of silicon ($\varepsilon = 11.7$), it is about 30% due to the larger dielectric constant. For a proof of the principle accelerating structure, we considered both materials. Table I shows the basic geometry parameters of such accelerating structures.

Another practical consideration of this accelerating structure design is an injection of a broadband THz pulse into a multicell structure of a broadband waveguide. Metal walls of the quasiplanar waveguides can be sharpened to create a tapered transition from vacuum into the structure.

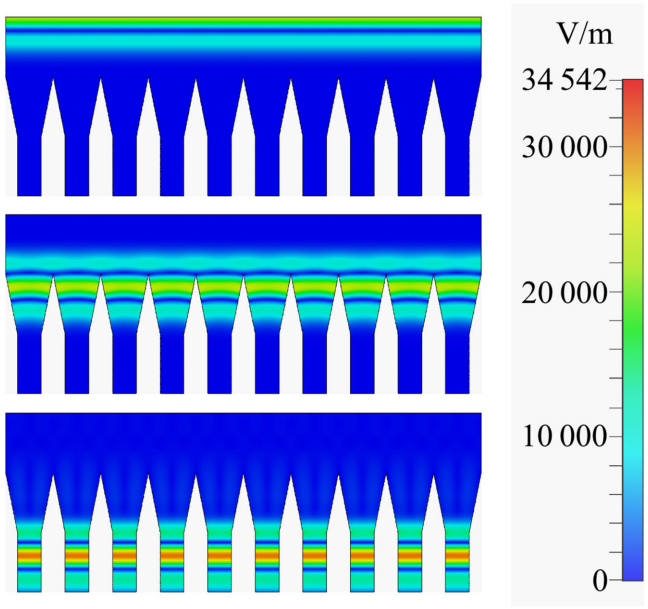

FIG. 10. Time snapshots of thereflection from the structure/vacuum interface.

Such a horn-antenna geometry allows for broadband matching of the short THz pulse. Simulation results in Fig. 10 show a small reflection from the entrance to the multicell structure described above. There is virtually no reflection at the entrance of the waveguide's horn-antenna-like apertures. Our simulations show −25 dB loss over the full spectrum, i.e., < 1% of the power.

We simulated particle acceleration in the quartz-delay-focusing-line multicell accelerating structure. This simulation was done in CST Microwave Studio [32]. We assumed a 3-MeV bunch of electrons with a 1-pC charge. The electron beam duration is 100 fs and the transverse size is 100 μm, which is typical for the state of high quality photoinjectors [33]. The structure has ten cells with appropriate delay lines. In our simulation, we assumed a 100 μJ THz pulse with the time structure and spectrum depicted in Fig. 1 delivered into accelerating cells. Considering all losses—reflection at the entrance, 0.5%, reflection at the delay line (11% for quartz), and power attenuation in the delay line and lens (4% for quartz)—the input energy of the pulse should be 116 μJ. With a total of 10 μJ per cell maximum, the accelerating field reaches 385 MV/m. Figure 11(a) shows the energy gain of the beam synchronous with the THz pulse as it travels through the structure at different time frames. The total energy gain is 600 keV [Fig. 11(b)]. The timing between the THz pulse and the electron beam was adjusted so that the maximum field in the accelerating cell was produced when the beam was in the middle of the cell.

Figure 12 shows accelerating structure parameter optimization scans. In Fig. 12(a), a phase injection scan is shown for different initial electron energies. Figure 12(b)

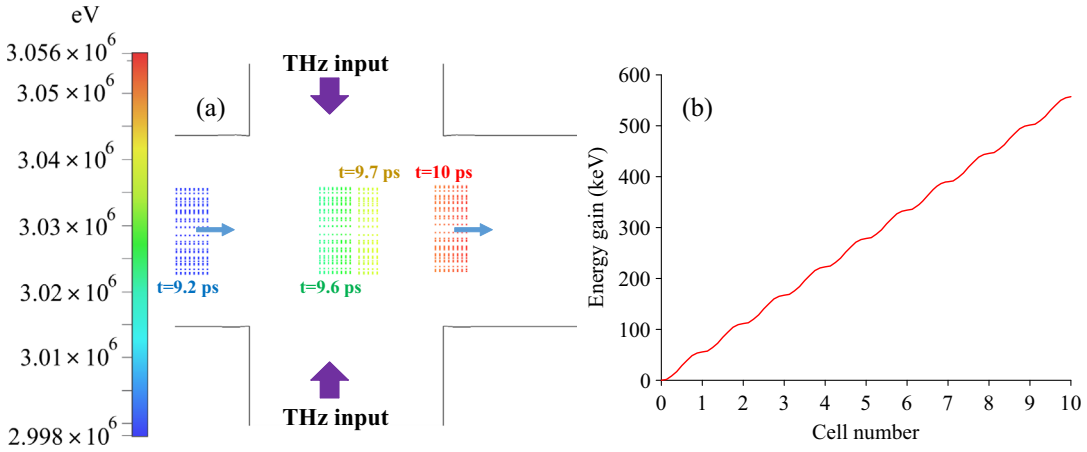

FIG. 11. Bunch acceleration in the structure: (a) Bunch acceleration for sequent time frames. (b) Cumulative energy gain along the beam path.

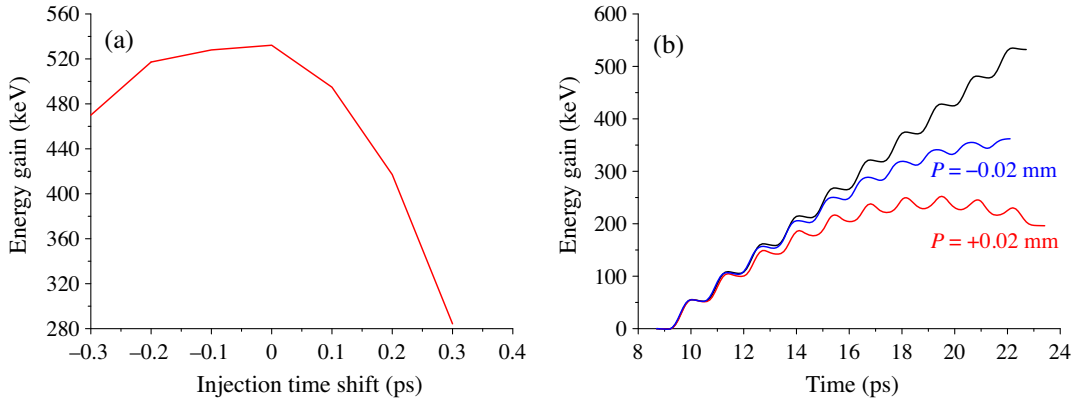

FIG. 12. Parameter optimization scans. (a) Energy gain as a function of injection time. (b) Energy gain as a function of structure periodicity.

illustrates energy gain changes as a function of the accelerating period length.

In the design and simulation of this accelerating structure, we considered all possible losses. We show that an effective long-range interaction between a broadband THz pulse and electron beam can be achieved. This approach can be used for manipulation of, for example, an ultrafast electron microscope beam: beam compression, energy chirping, or modulation.

IV. PROTOTYPE FABRICATION

We have produced silicon delay lines with lenses using laser microfabrication. The same method is compatible with lenses fabricated out of quartz. Figure 13 shows confocal scanning laser microscopy measurement results of the laser-cut silicon lens (black) sitting on a copper plate (orange/copper) with dimensional measurements of the sample units. The measurement is done by the Keyence VK-X1000 [34] microscope that combines laser scanning and optical measurement, hence the realistic colors for cut silicon wafer and copper backing. By stacking together such units (one unit = silicon lens + copper backing plate), one obtains a multicell accelerating structure as in Fig. 9. Figure 13(a) shows the 3D measurement view of the

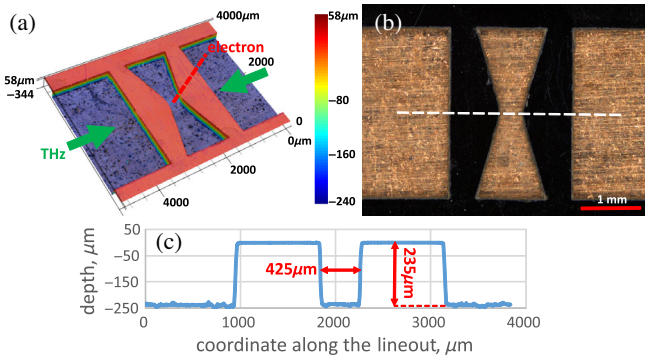

FIG. 13. (a) 3D scanning microscope metrology of the fabricated structure. THz input and electron trajectory are schematically shown. (b) Optical image of the structure with depth profile lineout shown. (c) Depth profile along the lineout from (b).

two-port silicon lens integrated with a delay line. The THz input (blue) and electron beam trajectory (red) are schematically depicted. This prototype was made to verify the laser cutting accuracy for silicon; there is no beam hole for electrons in copper. Such beam holes will be laser drilled for the experimental device. 3D measurement is done with a laser scanning confocal microscope. Figure 13(c) shows the dimensions of the lens thickness and spacing between lenses along the blue line shown in Fig. 13(b). The accuracy of such a fabrication method is on the order of 1 μm for linear dimensions. The surface roughness after laser ablation is 250–400 nm Sa. This is fully acceptable for THz electromagnetic structures, as the wavelength at 1 THz is 300 μm, i.e., significantly larger than surface roughness and dimensional accuracy.

V. CONCLUSION AND OUTLOOK

In this paper, we have presented a practical approach for electron acceleration with intense and short THz pulses. We utilize a dielectric lens embedded in a delay line to achieve a dispersion less focusing of the THz pulse. This allows us to achieve a high accelerating gradient and an appropriate field configuration for charged particle acceleration. Long-range interaction is achieved by stacking such accelerating cells together and timing the THz pulse arrival with respect to the electron beam travel by means of delay lines. The described structural prototype has been laser machined and proper dimensions have been produced. Such broadband accelerating structures may produce the highest-yet-achieved accelerating gradients in nonplasma accelerators due to ultrashort pulse duration.

[1] W. Wuensch, High-gradient X-band technology: From TeV colliders to light sources and more, CERN Courier (2018), https://cerncourier.com/a/high-gradient-x-band-technology-from-tev-colliders-to-light-sources-and-more/.

[2] S. G. Tantawi, V. Dolgashev, Y. Higashi, B. Spataro, S. H. Gold, and G. S. Nusinovich, Research and development for ultra-high gradient accelerator structures, AIP Conf. Proc. **1299**, 29 (2010).

[3] D. Broemmelsiek *et al.*, Record high-gradient SRF beam acceleration at Fermilab, New J. Phys. **20**, 113018 (2018).

[4] M. Litos *et al.*, High-efficiency acceleration of an electron beam in a plasma wakefield accelerator, Nature (London) **515**, 92 (2014).

[5] B. O'Shea, G. Andonian, S. Barber *et al.*, Observation of acceleration and deceleration in gigaelectron-volt-per-metre gradient dielectric wakefield accelerators, Nat. Commun. **7**, 12763 (2016).

[6] W. Kilpatrick, Criterion for vacuum sparking designed to include both rf and dc, Rev. Sci. Instrum. **28**, 824 (1957).

[7] J. Wang and G. Loew, rf breakdown studies in copper electron linac structures, in *Proceedings of the 1989 Particle Accelerator Conference, Chicago, IL* (IEEE, New York, 1989), pp. 1137–1139.

[8] A. Grudiev, S. Calatroni, and W. Wuensch, New local field quantity describing the high gradient limit of accelerating structures, Phys. Rev. ST Accel. Beams **12**, 102001 (2009).

[9] Xiaowei Wu *et al.*, High-gradient breakdown studies of an X-band Compact Linear Collider prototype structure, Phys. Rev. ST Accel. Beams **20**, 052001 (2017)

[10] D. P. Pritzkau and R. H. Siemann, Experimental study of rf pulsed heating on oxygen free electronic copper, Phys. Rev. ST Accel. Beams **5**, 112002 (2002).

[11] V. Dolgashev, S. Tantawi, Y. Higashi, and B. Spataro, Geometric dependence of radio-frequency breakdown in normal conducting accelerating structures, Appl. Phys. Lett. **97**, 171501 (2010).

[12] Lisa Laurent, S. Tantawi, V. Dolgashev, C. Nantista, Y. Higashi, M. Aicheler, S. Heikkinen, and W. Wuensch, Experimental study of rf pulsed heating, Phys. Rev. ST Accel. Beams **14**, 041001 (2011).

[13] A. Degiovanni, W. Wuensch, and J. G. Navarro. Comparison of the conditioning of high gradient accelerating structures, Phys. Rev. Accel. Beams **19**, 032001 (2016).

[14] K. Nordlund and F. Djurabekova, Defect model for the dependence of breakdown rate on external electric fields, Phys. Rev. ST Accel. Beams **15**, 071002 (2012).

[15] S. V. Kuzikov and M. E. Plotkin, Model of thermal fatigue of a copper surface under the action of high-power microwaves, Radiophys. Quantum Electron. **50**, 885 (2007.

[16] The Compact Linear Collider (CLIC)—2018 Summary Report. Geneva, Switzerland, edited by P. N. Burrows *et al.*, Report No. CERN-2018-005-M, arXiv:1812.06018 (2018).

[17] Z. Wu, A. S. Fisher, J. Goodfellow, M. Fuchs, D. Daranciang, M. Hogan, H. Loos, and A. Lindenberg, Intense terahertz pulses from SLAC electron beams using coherent transition radiation, Rev. Sci. Instrum. **84**, 022701 (2013).

[18] C. Vicario, A. V. Ovchinnikov, S. I. Ashitkov, M. B. Agranat, V. E. Fortov, and C. P. Hauri, Generation of 0.9-mJ THz pulses in DSTMS pumped by a $Cr:Mg_2SiO_4$ laser, Opt. Lett. **39**, 6632 (2014).

[19] C. Vicario, M. Jazbinsek, A. V. Ovchinnikov, O.V. Chefonov, S. I. Ashitkov, M. B. Agranat, and C. P. Hauri, High efficiency THz generation in DSTMS, DAST and OH1 pumped by Cr:forsterite laser, Opt. Express **23**, 4573 (2015).

[20] J. A. Fulop *et al.*, Efficient generation of THz pulses with 0.4 mJ energy, in *CLEO: Science and Innovations, SW1F–5* (Optical Society of America, 2014), 10.1364/OE.22.020155.

[21] M. Hibberd *et al.*, Acceleration of relativistic beams using laser-generated terahertz pulses, Nat. Photonics **14**, 755 (2020).

[22] H. Tang *et al.*, Stable and Scalable Multistage Terahertz-Driven Particle Accelerator, Phys. Rev. Lett. **127**, 074801 (2021).

[23] W. Ronny Huang, Arya Fallahi, Xiaojun Wu, Huseyin Cankaya, Anne-Laure Calendron, Koustuban Ravi, Dongfang Zhang, Emilio A. Nanni, Kyung-Han Hong,

and Franz X. Kärtner, Terahertz-driven, all-optical electron gun, Optica **3**, 1209 (2016).

[24] D. Zhang, A. Fallahi, M. Hemmer, X. Wu, M. Fakhari, Y. Hua, H. Cankaya, A.-L. Calendron, L. E. Zapata, N. H. Matlis, and F. X. Kärtner, Segmented terahertz electron accelerator and manipulator (STEAM), Nat. Photonics **12**, 336 (2018).

[25] Dongfang Zhang *et al.*, Femtosecond phase control in high-field terahertz-driven ultrafast electron sources, Optica **6**, 872 (2019).

[26] Franz X. Kärtner, Terahertz accelerator based electron and x-ray sources, Terahertz Sci. Technol. **13**, 22 (2020).

[27] S. V. Kuzikov, A. E. Fedotov, N. Yu. Peskov, A. N. Stepanov, and A. A. Vikharev, Millimeter and submillimeter-wave, high-gradient accelerating structures, AIP Conf. Proc. **1812**, 060002 (2017).

[28] S. V. Kuzikov *et al.*, Quasi-optical THz accelerating structures, in *Proceedings of AAC2018 Workshop, 2018, Breckenridge, Colorado* (2018), 10.1109/AAC.2018.8659437.

[29] S. V. Kuzikov *et al.*, Single cycle terahertz acceleration structures, in *Proceedings of NAPAC2019 Conference, Lansing, MI, 2019* (2019), 10.18429/JACoW-NAPAC2019-WEPLO11.

[30] S. Silver, *Microwave Antenna Theory and Design*, MIT Radiation Laboratory Series Vol. 12 (McGraw-Hill, New York, 1949), Chap. 11.

[31] D. Grischkowsky, Søren Keiding, Martin van Exter, and Ch. Fattinger, Far-infrared time-domain spectroscopy with terahertz beams of dielectrics and semiconductors, J. Opt. Soc. Am. B **7**, 2006 (1990).

[32] www.cst.com.

[33] F. Qi, Z. Ma, L. Zhao, Y. Cheng, W. Jiang, C. Lu, T. Jiang, D. Qian, Z. Wang, W. Zhang, P. Zhu, X. Zou, W. Wan, D. Xiang, and J. Zhang, Breaking 50 Femtosecond Resolution Barrier in MeV Ultrafast Electron Diffraction with a Double Bend Achromat Compressor, Phys. Rev. Lett. **124**, 134803 (2020).

[34] www.keyence.com/landing/lpc/laser-microscope-gss.jsp.